Nanoscale

PAPER

View Article Online
View Journal | View Issue

Cite this: *Nanoscale*, 2017, **9**, 4544

Ultrafast pressure sensing with transient tunnelling currents†

Ashok S. Chauhan, Isaac Taylor-Harrod, Samuel D. Littlejohn and Alain Nogaret*

Received 17th February 2017,
Accepted 10th March 2017

DOI: 10.1039/c7nr01214d

rsc.li/nanoscale

We report and systematically study large amplitude piezoresistance spikes in thin composite films under stress. These spikes are characterized by a unique double exponential decay which we demonstrate to be the signature of transient tunnelling currents. We establish an expression that predicts the dynamic conductivity of the composite with only three material parameters and use it to infer the magnitude of applied stress from resistance spikes, thus achieving quasi-instantaneous readout unhindered by viscoelastic relaxation. We demonstrate the proof of principle of ultrafast mechanoreceptors based on this effect by making a sensor array which images pressure at close to cinematic speeds with a sensitivity of 50 Pa.

Introduction

Mimicking the human touch with fast sensitive sensors is important for making intelligent human-machine interfaces,[1] biometric identification and pattern recognition systems,[2–4] biomimetic sensors,[5,6] biomedical implants,[7,8] and artificial skins that increase aerodynamic efficiency through active flow control.[9] Mechanoreceptors embedding graphitic nanoparticles,[10,11] carbon nanotubes,[12] graphene platelets,[13–15] in flexible polymer matrices rely on piezoresistance,[12,16–21] capacitance,[22,23] or piezoelectric[24] transduction to sense pressure. The viscoelastic nature of strain relaxation however severely limits the response times of organic conductors as internal stresses and strains stabilize long after deformation has been applied.[25,26] While nanoscale engineering helps reduce viscoelastic delays,[12] the short range intermolecular forces responsible for viscous relaxation can never be completely eliminated. This unavoidably hinders efforts to reduce the response time of pressure sensing polymers.[27,28]

Here, we demonstrate a dynamic method which makes constructive use of the instantaneous response of organic conductors to read strain and pressure on ultra-short time scales with high sensitivity. We establish the principle of this approach by interrogating an array of 64 × 64 sensors at a rate of 8 images per second with pressure resolution down to 50 Pa. The method relies on the formation of resistance spikes in organic films under stress. The spikes occur symmetrically during loading–unloading stress cycles. After each spike, the resistance recovers according to a double exponential decay which we demonstrate to be the signature of transient tunnelling currents. We perform a rigorous experimental and theoretical study of this effect in composites of highly oriented pyrolytic graphite (HOPG) nanoparticles in a polydimethylsiloxane (PDMS) matrix. By treating stress as a perturbation of sequential quantum tunnelling in the percolation network, we obtain a universal analytical formula which successfully predicts the dynamic piezoresistance with only three material parameters and which we use to rapidly and accurately infer stress from piezoresistance spikes.

Results and discussion

We performed time resolved electrical transport measurements in thin composite films. Our composites were prepared by mixing HOPG nanoparticles, of diameter d_{HOPG} = 450 nm in PDMS with volume filling fractions ranging from p = 22% to 34.2%. The composites were moulded and cured on cellulose acetate substrates to obtain conductive films 100 μm thick. Gold ohmic contacts were evaporated on the 8.0 mm long and 1.5 mm wide active region. The composite was incrementally stressed by bending the substrate with two purpose made stepper benches (ESI, sections 1 and 2†). The 4-terminal resistance was measured at a sampling rate of 20 kHz. Following a cycle of stress loading and stress unloading (Fig. 1a), the film resistance exhibits a series of sharp spikes followed by rapid recovery. After compression, the resistance decays towards a lower baseline which characterizes the partial recovery behaviour of non-ideal viscoelastic solids. Shortening the duration of individual stress steps from τ = 30 min to τ = 5 min changes the resistance profile from V-shaped (Fig. 1a) to M-shaped

Department of Physics, University of Bath, Bath, BA2 7AY, UK.
E-mail: A.R.Nogaret@bath.ac.uk

†Electronic supplementary information (ESI) available. See DOI: 10.1039/c7nr01214d

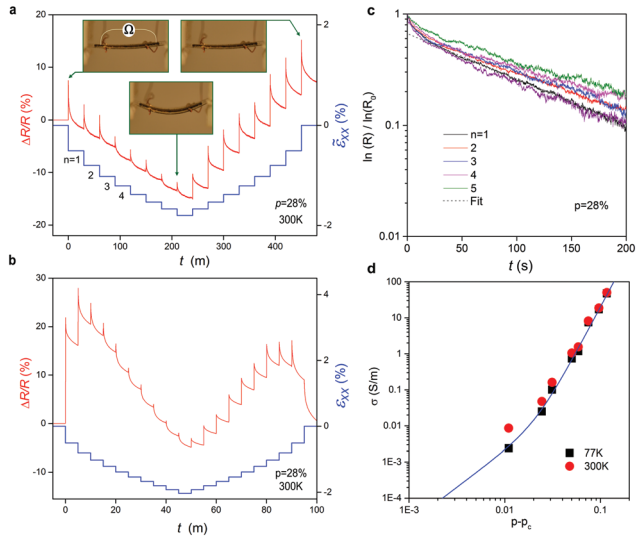

Fig. 1 Transient piezoresistance of composite thin films. (a) V-shaped resistance of thin films of HOPG–PDMS (red line) obtained by applying stress steps at intervals of τ = 30 min. During a compression–release cycle the cumulative strain (blue line) is calculated from incremental changes in the curvature radius (Table S5†). Inset: composite-acetate bilayer. (b) M-shaped resistance observed for τ = 5 min long intervals. (c) Decay of the thin film resistance in individual steps n = 1, 2, ..., 6 for HOPG filling fraction p = 28% (full lines). The decay is fitted with $R(t) \propto \exp(\exp(-t/\tau_c))$ using creep time τ_c = 240 s as the adjustment parameter (p = 28%) (dashed line). (d) Dependence of the percolation conductivity as a function of the HOPG filling fraction at 77 K (blue hollow squares) and 300 K (red dots). Data fitted using $\sigma = 20(p - p_c)^2 + 2 \times 10^6(p-p_c)^{4.7}$ give a percolation threshold p_c = 22.5%.

(Fig. 1b). The *dynamic* piezoresistance we observe is always positive when loading or unloading the composite. The rise time of piezoresistance spikes is of the order of the millisecond and their amplitude is reproducible within 8% for strain steps of small magnitude (<0.5%). After each spike, the resistance recovers according to a double exponential time dependence, of the form $R(t) \propto \exp[\exp(-t/\tau_c)]$ (Fig. 1c). The fit of the resistance decay in films with p = 28% filling fraction (resp. p = 31%) gives decay time τ_c = 240 ± 25 s (resp. 175 ± 25 s). The *I–V* curves of the bilayer are linear (Fig. S6†). Their d.c. conductivity at zero-bias was plotted as a function of HOPG filling fraction in Fig. 1d (symbols). One verifies that the conductivity increases as a power law of the HOPG filling fraction, $\sigma = \sigma_0(p - p_c)^\alpha$, which characterizes percolation transport (full line). The fit to the data gives a percolation threshold: p_c = 22.5%, α = 4.7, and $\sigma_0 = 2 \times 10^6$ S m^{-1}.

In order to describe the piezoresistance spikes, we model percolation transport by calculating the sequential tunnelling current through percolation bonds randomly oriented in the strain field generated by substrate bends. This picture follows from the observation of a double exponential decay law (Fig. 1c). The first exponential is associated with the dependence of the tunnelling current on the tunnelling barrier width in percolation links which undergo maximum elongation during *elastic* deformation. The second exponential arises from the exponential time dependence of the tunnelling bond length during the *viscous* recovery phase. Our theory goes beyond static effective medium approaches[27,28] by describing for the first time the dynamic conductivity of the viscoelastic solid. We begin by establishing the exact 3D stress and strain tensors induced by bending the substrate. Changing the radius of curvature of the substrate from ρ_{n-1} to ρ_n applies biaxial stress $(\Delta_n\sigma_{xx},\Delta_n\sigma_{yy},0)$ in the plane (Fig. 2a). The magnitude of the n^{th} stress increment is proportional to $\Delta_n(1/\rho) = \rho_n^{-1} - \rho_{n-1}^{-1}$. This stress induces a strain field $(\Delta_n\varepsilon_{xx},\Delta_n\varepsilon_{yy},\Delta_n\varepsilon_{zz})$ in the composite which is transmitted to HOPG nanoparticles *via* the *instantaneous elastic action* of viscoelastic coupling. Assuming the mechanical coupling between HOPG nanoparticles is described by a spring-dashpot model,[30] it follows that stress and strain will decay exponentially with respective time constants τ_R (stress relaxation time) and τ_c (creep time). Because the deformations involved are

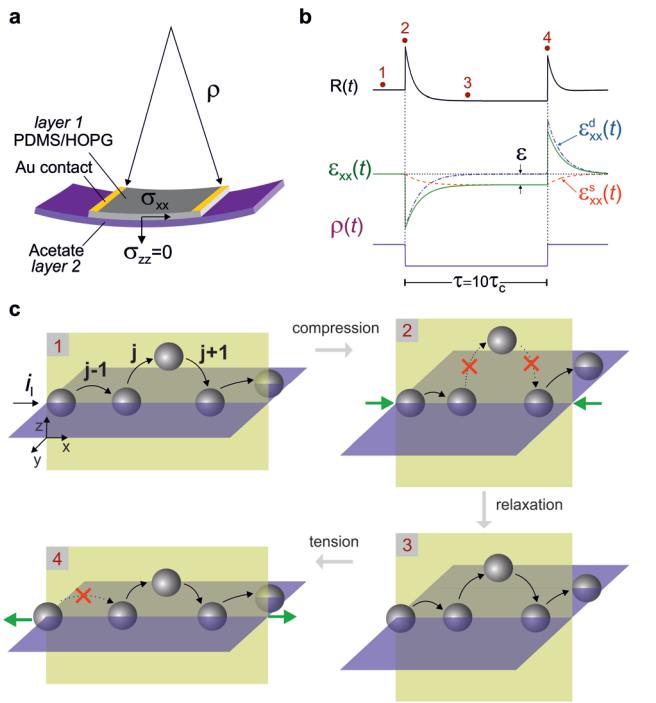

Fig. 2 Perturbative tunnelling model of the linear viscoelastic solid. (a) Stress is applied to the PDMS/HOPG composite film by bending the substrate. (b) Time dependence of the resistance (black line) and the longitudinal strain (green line) calculated for a consecutive decrease and increase in curvature radius (purple line). The longitudinal strain $\varepsilon_{xx}(t)$ is the sum of a monotonically increasing component, $\varepsilon_{xx}^s(t)$, which accounts for incomplete viscoelastic relaxation (red dashed line) and $\varepsilon_{xx}^d(t)$ which contains the stress spike (blue dashed dotted line). (c) Sequential tunnelling model. (1) At rest, percolation line l carries current i_l through bonds ..., j − 1, j, j + 1, ...; (2) compression along x instantaneously increases the length of tunnelling bonds in the z-direction which causes the first resistance spike; (3) bond lengths relax to a new average value over time scaleτ_c causing the resistance to drop; (4) unloading stress instantly increases bond lengths in the x-direction causing the second resistance spike.

small (<0.5%), strain may be calculated analytically within the linear response.[29] The strain tensor was calculated by solving the equations of linear viscoelasticity in the dynamic regime.[30] After the N^{th} change in curvature radius, the principal components of strain are:

$$\begin{cases} \varepsilon_{xx}(t) = -\dfrac{E_2}{6E_1}\dfrac{1-\gamma_1\gamma_2}{1-{\gamma_2}^2}\dfrac{{a_2}^3}{a_1(a_1+a_2)}\displaystyle\sum_{n=1}^{n=N}\Delta_n\left(\frac{1}{\rho}\right)H(t-n\tau)F(t,n), \\ \varepsilon_{yy}(t) = -\dfrac{E_2}{6E_1}\dfrac{\gamma_2-\gamma_1}{1-{\gamma_2}^2}\dfrac{{a_2}^3}{a_1(a_1+a_2)}\displaystyle\sum_{n=1}^{n=N}\Delta_n\left(\frac{1}{\rho}\right)H(t-n\tau)F(t,n), \\ \varepsilon_{zz}(t) = +\dfrac{E_2}{6E_1}\dfrac{\gamma_1(1+\gamma_2)}{1-{\gamma_2}^2}\dfrac{{a_2}^3}{a_1(a_1+a_2)}\displaystyle\sum_{n=1}^{n=N}\Delta_n\left(\frac{1}{\rho}\right)H(t-n\tau)F(t,n), \end{cases}$$

$$\text{where}\quad F(t,n) = \left[\exp\left(-\frac{t-n\tau}{\tau_c}\right) + \varepsilon\frac{\tau_c}{\tau_R}\left(1-\exp\left(-\frac{t-n\tau}{\tau_c}\right)\right)\right], \tag{1}$$

and E_1 (resp. E_2), γ_1 (resp. γ_2), a_1 (resp. a_2) are the Young's modulus, Poisson ratio and thickness of the composite (resp. substrate), $H(t)$ is the Heaviside step function, τ is the time interval between bends and ε is the partial stress relaxation ratio which accounts for incomplete stress relaxation in the non-ideal viscoelastic solid ($0 < \varepsilon < 1$). The time dependence of strain $F(t, n)$ in eqn (1) is the sum of two components: a dynamic strain ${\varepsilon_{\mu\mu}}^d(t)$ ($\mu \equiv x,y$) which *decays to zero* at long times as described by the first term in $F(t, n)$, and a static strain ${\varepsilon_{\mu\mu}}^s(t)$ which *increases* until a saturation level proportional to the partial recovery ratio ε – second term in $F(t, n)$. The time dependence of these two strain components is plotted in Fig. 2b. Note that the amplitude of a strain spike, in eqn (1), is proportional to the stress increment $\Delta_n\sigma_{xx}$. Eqn (1) also prescribes that bending the substrate, $\Delta_n(1/\rho) > 0$, has the effect of shrinking the composite film in the *x*-direction and expanding it in the *z*- and *y*-directions.[27] At the microscopic level, the width of a tunnelling barrier between two nanoparticles increases or decreases depending of its orientation in the strain field (eqn (1)), and stress loading or unloading. For example, under compression, bonds oriented in the *z*- and *y*-directions will expand. This will increase the overall resistance of the percolation line. If instead the composite is stretched, bonds oriented along the *x*-axis will expand and become the weakest links of the percolation chain. Macroscopically, the piezoresistance is therefore positive under both tension and compression (Fig. 2b). This qualitatively explains the symmetry of the piezoresistance spikes observed through loading–unloading cycles in Fig. 1. In a perfect elastomer ($\gamma_1 = 0.5$), deformation occurs at constant volume: $\varepsilon_{xx} + \varepsilon_{yy} + \varepsilon_{zz} = 0$ which one also verifies in eqn (1).

Next, the dynamic piezoresistance is calculated by considering stress as a perturbation of the steady state resistance of the percolation network. The amplitude of stress steps (Table S5†) is small enough that stress does not change the topology of the percolation network. The effect of stress is only to change the length of tunnelling bonds depending on their orientation relative to the strain field of eqn (1). The low bias tunnelling current density through bond *j* of percolation line *l* (Fig. 2c) is given by Simmons[31] as $i_l \propto \frac{\sqrt{V_0}}{b_{jl}} V_{jl}\exp(-\kappa b_{jl})$ where V_0 is the height of the PDMS potential barrier, b_{jl} is the barrier width and $\kappa = 2\sqrt{2m \times V_0/\hbar^2}$. We obtain the resistance of the composite film by applying Kirchhoff's voltage law to voltages V_{jl} dropped across the bonds of current line *l*, and Kirchhoff's current law to all current lines through the composite. We make the assumption that, at rest, all tunnelling bonds have equal length $b_{jl} = b_0$. It may be shown that the most conductive (hence likeliest) percolation path is the one for which all connections have lengths equal to the tunnelling length $b_0 = \kappa^{-1}$. When stress is applied, incomplete viscoelastic relaxation – under the effect of ${\varepsilon_{\mu\mu}}^s(t)$ – changes the *average* bond length from b_0 to b. In addition, the ${\varepsilon_{\mu\mu}}^d(t)$ term induces a *relative* change in bond length Δb_{jl}. Δb_{jl} depends on the orientation of bonds in the strain field which is random hence can be positive or negative. We calculated the dynamic resistance perturbatively by substituting b_0 with $b + \Delta b_{jl}$ in the resistance of the composite. Retaining the first order terms in Δb_{jl}, the dynamic resistance may be written as the product of two terms: a slowly varying resistance term, $R_0(t)$, associated with viscoelastic relaxation of the tunnelling barrier average b; and a rapidly varying term accounting for direction dependent changes in tunnelling probabilities. The second term is responsible for the resistance spikes. Due to the large number of bonds ($\sim 10^4$) in a percolation path, one may write the sum over bonds b_{jl} as a continuous sum over the 4π solid angle to obtain the time dependent resistance:

$$R(t) = R_0(t)\frac{1}{4\pi}\int_0^{2\pi}\mathrm{d}\varphi\int_0^{\pi}\mathrm{d}\theta\,\sin\theta \exp\left(\kappa b_0\frac{\Delta b(\theta,\varphi,t)}{b_0}\right)w(\theta,\varphi) \tag{2}$$

where:

$$R_0(t) = R_0\left[1-\frac{3p}{p-p_c}\left(1-\left(\frac{6p}{\pi}\right)^{1/3}\right)\alpha{\varepsilon_{xx}}^s(t)\right]$$

and:

$$\frac{\Delta b(\theta,\varphi,t)}{b_0} \cong {\varepsilon_{xx}}^d(t)\,\sin^2\theta\cos^2\varphi + {\varepsilon_{yy}}^d(t)\,\sin^2\theta\sin^2\varphi + {\varepsilon_{zz}}^d(t)\,\cos^2\theta$$

Setting the weight function as $w(\theta, \varphi) = 1$ models random hopping whereas $w(\theta, \varphi) = 2\sin\theta\cos\varphi$ models directional hopping driven by bias along the *x*-direction. Random hopping correctly predicts the symmetric piezoresistance observed in Fig. 1 over a loading–unloading cycle (ESI, Fig. S7†). In contrast, an asymmetric piezoresistance is observed when directional hopping is considered (ESI, Fig. S7†). This argument indicates that percolation proceeds by random hopping through the isotropic network.

We now validate the theory by comparing its predictions to the experiment. Eqn (2) demonstrates that the double exponential decay of the piezoresistance (Fig. 1c) arises from expo-

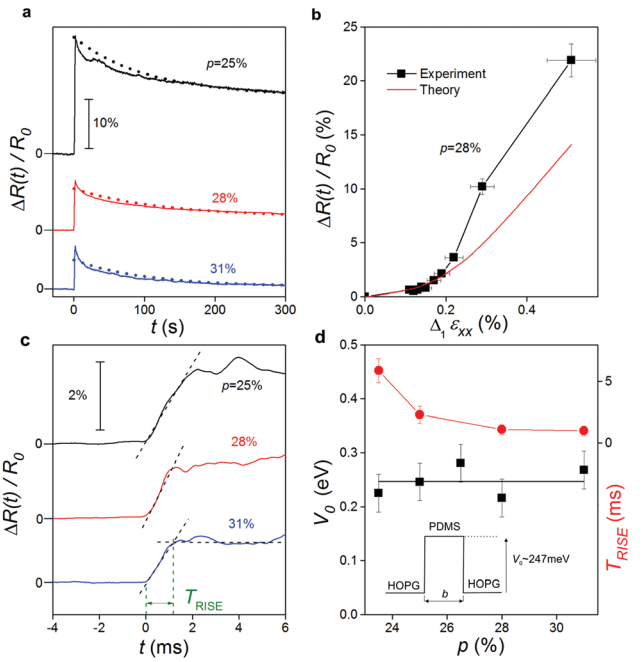

Fig. 3 Experimental results. (a) Dependence of the resistance spike amplitude on the HOPG filling fraction (full lines) and theoretical fits with eqn (2) (dotted lines). (b) Dependence of the spike amplitude on applied strain: experiment (square symbols) theoretical prediction (red line). (c) Time resolved response of the spike rise time. (d) Dependence of the tunnelling barrier height V_0 and the rise time of the piezoresistance T_{rise} on the HOPG filling fraction. The former is fitted from panel (a), the latter from panel (c).

nential relaxation of PDMS bond lengths over time, combined with the exponential dependence of tunnelling on bond length. Eqn (2) was used in Fig. 3a (dashed lines) to fit the amplitudes of resistance spike $n = 1$ for different HOPG filling fractions. These fits give the values of material parameters $V_0 = 247 \pm 21$ meV, $\varepsilon = 0.15$ and $\tau_c = 240$ s. Incorporating these parameters into eqn (2) allows us to predict the dependence of the resistance spike amplitude (dynamic piezoresistance) when a strain step is applied (Fig. 3b, red line). The theoretically predicted piezoresistance is in good agreement with experimental observation (symbols). Therefore eqn (2) may be used to accurately infer strain from the amplitude of resistance spikes in sensor devices. At low values of strain, $\Delta_1\varepsilon_{xx} < 0.2\%$, a gauge factor of 8 may be inferred from the linear dependence of the piezoresistance on strain. Discrepancies between experiment and theory at higher strain may be ascribed to a limitation of our perturbative approach which gives the highest accuracy at small strains. Fig. 3c plots time resolved measurements of the rising front of the $n = 1$ resistance spike. The piezoresistance rise time is found to be $T_{rise} \approx 1$ ms for $p = 28\%$. The dependence of T_{rise} on the filling fraction is shown in Fig. 3d where T_{rise} increases when p decreases. The other parameters, V_0, τ_c, and ε are, within experimental error, all independent of the HOPG filling fraction, as expected from intrinsic material parameters. Eqn (2) further correctly explains the M- and V-shapes of the piezoresistance in Fig. 1a & b. The M-shape arises from incomplete stress relaxation over stress steps of shorter duration $\tau \leq \tau_c$ (ESI, Fig. S8†). Eqn (2) also explains the effect of material parameters V_0, τ_c, and ε on the piezoresistance (ESI, Fig. S9–11†) which allow our findings to be generalized to other composite materials. There is no optimum filling fraction for sensing because the piezoresistance depends very little on p. This is shown experimentally in Fig. 3a and c and theoretically in Fig. S9.† The choice of HOPG filling fractions in the 25.6%–34.2% range happens to be practical. 34% is the threshold of miscibility of HOPG in PDMS. Above this level, the mixture forms lumps. Below 25.6% the resistance of the

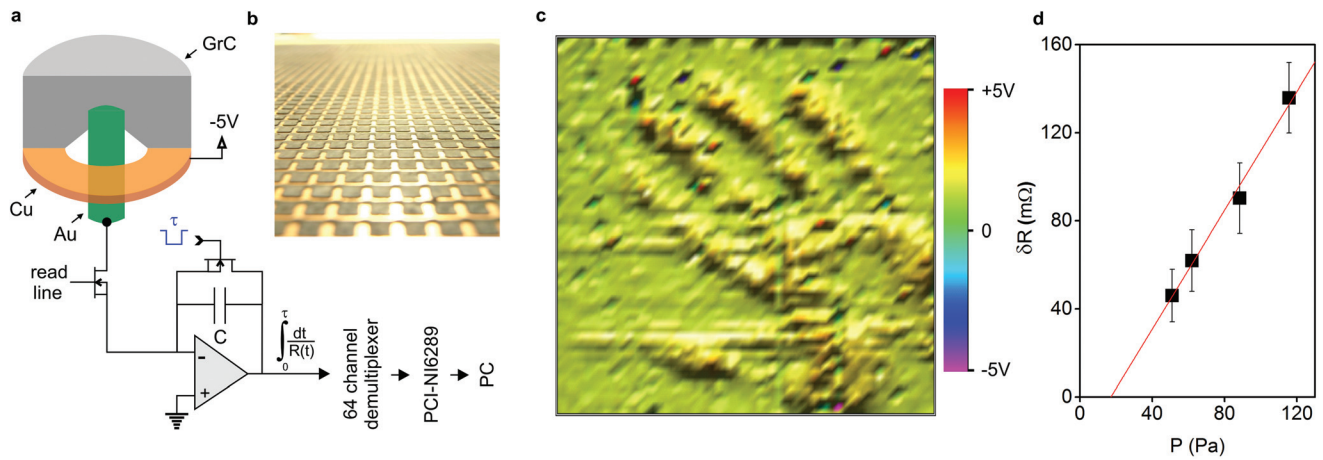

Fig. 4 Fast force field imaging with a 64 × 64 sensor array. (a) Each pixel in the array senses pressure by integrating the transient current passing through composite piezoresistor (GrC). The integration time was $\tau = 1$–7 ms depending on sampling rate. This is 5 orders of magnitude less than the viscoelastic relaxation time ($\tau \ll \tau_c$). (b) Detail of the sensor array showing individual piezoresistive elements pitched at 2.54 mm. The pixels in each row were read in parallel by a bank of 64 integrators which achieves 7 images per second. The readings of each row were demultiplexed and acquired by a DAQ card (PCI-NI6289) to generate a pressure map. (c) Image obtained by applying hand pressure on the sensor array. (d) Piezoresistance–pressure calibration curve obtained with integration time $\tau = 10$ ms.

composite increases in the MΩ range (Fig. S6†) which increases the signal-to-noise ratio of the sensor.

To demonstrate pressure imaging with the dynamic piezoresistance, we have built the sensor of Fig. 4a which integrates spikes over a time window comparable to the composite rise time, T_{rise}. A 64 × 64 sensor array (Fig. 4b; ESI,† section 6) was built to construct pixelated images of the pressure field with 0.1 inch spatial resolution. The 64 sensors in each row were scanned in parallel by a bank of 64 integrators which allowed the array to be interrogated at a frequency of up to 8 images per second. The array was used to visualize a pressure imprint in Fig. 4c. The pressure detection threshold was accurately estimated by immersing one sensor in water tank and applying acoustic pulses (3.5 MHz) of calibrated amplitude. The change in resistance observed near the pressure detection threshold is shown in Fig. 4d. The pressure sensitivity threshold is found to be ~50 Pa. This limit is set by instrument noise.

Conclusions

In summary, we have systematically studied the transient piezoresistance of thin composite films and found that strain and pressure may be reliably deduced from the amplitude of resistance spikes. We have derived the theoretical relationship between piezoresistance and stress that correctly predicts the experimental piezoresistance. This allows ultrafast pressure sensors to be made and calibrated. We demonstrated the feasibility of this approach by imaging time dependent pressure fields at close to cinematic speeds with a 4096 sensor array. The proposed sensing method may be extended to other conductive elastomers by using appropriate values for V_0, ε, τ_c.

Experimental

Material preparation

The composites were prepared by mixing HOPG nanoparticles (450 nm NanoAmor) in dimethylpolysiloxane (Alchemie RTV137) in volume fractions ranging from 22% to 34.2% (Fig. S13†). Once the mixture became homogeneous, after 15 min of continuous mixing with pestle and mortar, catalyst C137 was added. The mixture was coated on cellulose acetate substrate to form thin strips (100 μm thick, 5 mm wide, 8 mm long) and left to cure for 96 hours at room temperature (Fig. S14†). Au contacts were thermally evaporated at the ends of the strip (Fig. S15†). The contact resistance (~15 Ω) was negligible compared to the resistance of the composite which varied between 1 kΩ and 50 kΩ depending of the HOPG volume filling fraction. Labelling the composite film as layer 1 and the acetate substrate as layer 2 (Fig. S3†), the bilayer has the following parameters: thickness a_1 = 100 μm (a_2 = 100 μm); Young's modulus, E_1 = 1.8 ± 0.05 MPa (E_2 = 41 ± 11 MPa); Poisson ratio, γ_1 = 0.4999 ± 0.0001 (γ_2 = 0.391 ± 0.008).

Experimental setup

Piezoresistance measurements. Stress cycles were applied by bending the bilayer with a purpose made linear actuator controlled by a stepper motor (Fig. S1†). Its 0.5 mm pitch shaft screw displaced clamps horizontally in steps of 200 ± 1 μm monitored by a dial gauge. The bilayer was pinned at both ends by grooves micromachined at 70 degrees to avoid imparting a torque. A Labview program recorded the 4-terminal resistance with a digital multimeter while changing the curvature radius of the bilayer at set time intervals. The rise time of the piezoresistance was measured with the piezoceramic actuator bench shown in Fig. S2.† The actuator (Piezo systems, PSI-5A4E) had a 1 μs response time. The voltage was acquired by a DAQ card (NI-PCI6289) at a sampling rate of 20 kHz.

Pressure mapping. A 64 × 64 sensor array was built which generated images of applied pressure by integrating the current variation induced by resistance spikes (Fig. S12†).

Acknowledgements

This work has been supported by DSTL under grants CDE 32154 and CDE 28143 and EPSRC DTA studentships (ITH & SDL). We thank Prof. C. R. Bowen for the loan of piezoceramic actuators.

Notes and references

1 Y. Zhang, F. Zhang, C.-A. Di and D. Zhu, *Mater. Horiz.*, 2015, **2**, 140.
2 R. A. Potyrailo and A. M. Leach, *Appl. Phys. Lett.*, 2006, **88**, 134110.
3 X. Wang, Y. Gu, Z. Xion, Z. Cui and T. Zhang, *Adv. Mater.*, 2014, **26**, 1336–1342.
4 J. W. Wang, Z. S. Yao, T. Lei and A. W. Poon, *Sci. Rep.*, 2014, **4**, 7528.
5 D. Kang, P. V. Pikhitsa, Y. W. Choi, C. Lee, S. S. Shin, L. Piao, B. Park, K.-Y. Suh, T.-I. Kim and M. Choi, *Nature*, 2014, **516**, 222.
6 S. Littlejohn, A. Nogaret, G. M. Prentice and G. D. Pantoș, *Adv. Funct. Mater.*, 2013, **23**, 5398.
7 M. S. Humayun, J. D. Weiland, G. Y. Fuji, R. Greenberg, R. Williamson, J. Little, B. Mech, V. Cimmarusti, G. Van Boemel, G. Dagnelie and E. de Juan Jr., *Vision Res.*, 2003, **43**, 2573.
8 B. Olshansky, M. Richards, A. Sharma, N. Wold, P. Jones, D. Perschbacher and B. L. Wilkoff, *Circ.: Arrhythmia Electrophysiol.*, 2016, **9**(8), e003806.
9 M. Gad El Hak, *Act. Flow Control*, 2007, **95**, 1.
10 T. Someya, T. Sekitani, S. Iba, Y. Kato, H. Kawaguchi and T. Sakurai, *Proc. Natl. Acad. Sci. U. S. A.*, 2004, **101**, 9966.
11 T. Someya, Y. Kato, T. Sekitani, S. Ina, Y. Noguchi, Y. Murase, H. Kawaguchi and T. Sakurai, *Proc. Natl. Acad. Sci. U. S. A.*, 2005, **102**, 12321.

12 D. J. Lipomi, M. Vosgueritchian, B. C. T. Tee, S. Hellstrom, J. A. Lee, C. H. Fox and Z. Bao, *Nat. Nanotechnol.*, 2011, **6**, 788.
13 C. You, T. Huang, H. Wang, H. Yu, Q. Zhang and Y. Yaogang, *Sci. Rep.*, 2013, **3**, 3138.
14 L. Chen, G. Chen and L. Lu, *Adv. Funct. Mater.*, 2007, **17**, 898.
15 T. Ramanathan, A. A. Abdala, S. Stankovich, D. A. Dikin, M. Herrera-Alonso, R. D. Piner, D. H. Adamson, H. C. Schniepp, X. Chen, R. S. Ruoff, S. T. Nguyen, I. A. Aksay, R. K. Prudhomme and L. C. Brinson, *Nat. Nanotechnol.*, 2008, **3**, 328.
16 M. Ying, A. P. Bonifas, N. Lu, Y. Su, R. Li, H. Cheng, A. Ameen, Y. Huang and J. A. Rogers, *Nanotechnology*, 2012, **23**, 344004.
17 S. Littlejohn, A. Nogaret and S. Crampin, *Adv. Mater.*, 2011, **23**, 2815.
18 X. Wang, Y. Gu, Z. Xiong, Z. Cui and T. Zhang, *Adv. Mater.*, 2013, **26**, 1336.
19 K. Takei, T. Takahashi, J. C. Ho, H. Ko, A. Gillies, P. Leu, R. S. Fearing and A. Javey, *Nat. Mater.*, 2012, **7**, 825.
20 S.-E. Zhu, M. Krishna Ghatkesar, C. Zhang and G. C. A. M. Janssen, *Appl. Phys. Lett.*, 2013, **102**, 161904.
21 W. Wu, X. Wen and Z. Li Wang, *Science*, 2014, **340**, 952.
22 S. C. B. Mannsfeld, B. C.-K. Tee, R. M. Stoltenberg, C. V. H.-H. Chen, S. Barman, B. V. O. Muir, A. N. Sokolov, C. Reese and Z. Bao, *Nat. Mater.*, 2010, **9**, 859.
23 J. Kim, T. Nga Ng and W. Soo Kim, *Appl. Phys. Lett.*, 2012, **101**, 103308.
24 T. Q. Trung, N. T. Tien, Y. G. Seol and N.-E. Lee, *Org. Electron.*, 2012, **13**, 533.
25 Y. Ishigure, S. Iijima, H. Ito, T. Ota, H. Unuma, M. Takahashi, Y. Hikichi and H. Suzuki, *J. Mater. Sci.*, 1999, **34**, 2979.
26 S. Stassi, V. Cauda, G. Canavese and C. F. Pirri, *Sensors*, 2014, **14**, 5296.
27 D. A. G. Bruggeman, *Ann. Phys.*, 1935, **24**, 636.
28 R. Landauer, *J. Appl. Phys.*, 1952, **23**, 779.
29 M. Ohring, in *Materials Science of Thin films*, ed. M. Ohring, Academic Press, 2002, pp. 711–781.
30 S. C. Hunter, *Mechanics of Continuous Media*, John Wiley, ch. 15, 1976.
31 J. G. Simmons, *J. Appl. Phys.*, 1963, **34**, 238; J. G. Simmons, *J. Appl. Phys.*, 1963, **34**, 1793.